NASA CONTRACTOR REPORT 166452

Evaluation of Truncation Error and Adaptive Grid Generation for the Transonic Full Potential Flow Calculations

S. Nakamura

CONTRACT NCA2-OR565-101
February 1983

NASA

NASA CONTRACTOR REPORT 166452

Evaluation of Truncation Error and Adaptive Grid Generation for the Transonic Full Potential Flow Calculations

S. Nakamura
Ohio State University
Columbus, Ohio 43210

Prepared for
Ames Research Center
Under Grant NCA2-OR565-101

National Aeronautics and
Space Administration

Ames Research Center
Moffett Field, California 94035

EVALUATION OF TRUNCATION ERROR AND ADAPTIVE GRID GENERATION FOR THE TRANSONIC FULL POTENTIAL FLOW CALCLATIONS

S. Nakamura
Mechanical Engineering Department
The Ohio State University
208 West 18th Avenue
Columbus, Ohio 43210

1. INTRODUCTION

In solving the transonic full potential equations by using finite difference approximations on a transformed coordinate system, the solution is affected by the following four kinds of numerical errors:

(1) numerical error in evaluating the metrics of the coordinates,

(2) error due to discretization of the full potential equation,

(3) error due to artificial viscosity for the supersonic domain, and

(4) error due to approximating the shock behavior on the grids with finite spacing.

When a numerical grid generation method is used, the matrics of the transformation are calculated by finite difference approximations using the coordinates of the grids, so they are subject to errors, which in turn affect the accuracy of the finite difference approximation of the flow equation on the transformed coordinates. The error due to discretization is attributed to the truncation error of the finite difference approximation of the flow equation and becomes larger as the partial derivatives of the flow potential distribution become larger. The artificial viscosity is used to stabilize the iterative convergence of the transonic full potential equations, but introduces errors in the solution. Although the error in the numerical solution and the truncation error are related to each other in a very complicated manner, the error of the solution decreases when the truncation errors of the difference approximation in both the metric calculation and the flow solution

decrease. Naturally it is desirable to increase the number of grids in the areas of the flow domain where the truncation error is likely to be high.

Recent studies [1-3] on the use of adaptive grids for transonic full potential flow computations indicate that computing efficiency in terms of accuracy and cost is substantially improved by using adaptive grids. In those studies, the computations proceed in the following four steps: (1) generation of initial grids, (2) solution of the full potential equation on the initial grids (initial flow solution), (3) generation of adaptive grids using the information from the initial flow solution, and (4) flow solution on the adpative grids (adaptive grid flow solution). In generating adaptive grids, the locations of the supersonic bubble, the location of shock, and the area of high flow acceralation are identified from the initial flow solution.

In order to further develop the adaptive grid procedure, however, two major questions should be answered. First, what information from the solution on the initial grids should be used in generating the adaptive grids, and second, how to allocate the total number of grids available in the entire flow domain in such a way that the overall accuracy of the solution becomes optimized. Although these problems were investigated in recent studies [4,5], no clear answers have been obtained in conjunction with the full potential flow calculations.

The objectives of the present study are (1) to investigate the feasibility of using an estimate of the truncation error of the difference equation as a measure for the quality of the grids, (2) to investigate what information from the initial solution should be used in generating adaptive grids, and (3) the effect of irregularity of grid spacings.

For the sake of simplicity, our effort in this study is focused on the grid distribution along the airfoil surface. Furthermore, the numerical investigation is performed by solving the full potential equation on the Cartesian coordinates for a symmetric parabolic arc airfoil. Use of coordinate transformation is avoided so that the study can be done without being affected by the numerical error of the metrics of the transformation. Therefore, the airfoil boundary condition in the numerical study is represented along a straight line as a thin airfoil

perturbation.

2. TRUNCATION ERROR ALONG THE AIRFOIL SURFACE

In this section, the effect of grid spacing on the truncation error of a finite difference approximation for the two-dimensional full potential equation on the Cartesian coordinates is analytically studied. The full potential equation is written as

$$(R(F_x))_x + (R(F_y))_y = 0 \qquad (1)$$

where F is the potential fuction and R is the fluid density. We proceed the derivation of the truncation error expressions for the following cases: (A) R=1 (flow is assumed to be incompressible) and constant grid spacing, (B) R=1 (incompressible flow) and variable grid spacing, (C) compressible subsonic flow with variable grid spacing (R is variable) , and (D) supersonic flow with variable grid spacing. In the remainder of this report, only the truncation error of the difference approximation for the first term of Eq.(1) along the airfoil surface will be considered.

(A) Truncation Error for Incompressible Flow on Equally Spaced Grids

With R=1 and equally spaced grids on the x-coordinate, the difference approximation for the first term of Eq.(1) is written as

$$\delta^2 F/\delta x^2 = (F_{i-1,j} - 2F_{i,j} + F_{i+1,j})/h^2 \qquad (2)$$

By applying the Taylor expansion to $F_{i-1,j}$ and $F_{i+1,j}$, Eq.(2) becomes

$$\delta^2 F/\delta x^2 = F_{xx} + (1/12)h^2 F^{iv} + (1/360)h^4 F^{vi} + \ldots \qquad (3)$$

where h is the grid spacing and F^n is the n-th partial derivative of F with respect to x. Equation (3) shows that the truncation error is represented by

$$TE(x) = \delta^2 F/\delta x^2 - F_{xx} \approx (1/12)h^2 F^{iv} \qquad (4)$$

which is second-order in h.

(B) Truncation Error for Incompressible Flow on Nonuniform Grids

Using the three grids at x-g, x, and x+h, respectively, the three-point second order difference approximation for the first term of Eq.(1) is written as

$$\delta^2 F/\delta x^2 = \frac{[F(x+h)-F(x)]/h - [F(x)-F(x-g)]/g}{(g+h)/2} \qquad (5)$$

Using the Taylor series expansion, the truncation error is written as

$$TE(x) = \delta^2 F/\delta x^2 - F_{xx}$$

$$= (1/3)(h-g)F''' + (h^2/12)\frac{((g/h)^3+1}{g/h+1}F^{iv} + \ldots \qquad (6)$$

The above equation shows that, if g≠h, the truncation error is proportional to (h-g), indicating that a rapid change of grid spacing causes a significant amount of truncation error.

(C) Truncation Error for Subsonic Compressible FLow on Nonuniform Grids

The difference approximation for the first term of Eq.(1) on nonuniformly spaced grids may be written as

$$\frac{1}{(g+h)/2}\left[R_{i+1/2}\frac{F_{i+1}-F_i}{h} - R_{i-1/2}\frac{F_i-F_{i-1}}{g}\right] \qquad (7)$$

where g and h are the grid spacings defined in (B). The truncation error of Eq.(7) may be found by introducing Taylor series expansion of $R_{i+1,j}$ and $F_{i+1,j}$ about x_i into Eq.(7) and subtracting the first term of Eq.(1). After a manipulation of the terms, the lowest terms in the truncation error are found as

$$TE(x) =$$

$$+ (h-g)\left[(1/16)R_i''F_i' + (1/4)R_i'F_i'' + (1/3)R_iF_i'''\right]$$

$$+ \left[\frac{g^3+h^3}{96(g+h)}R'''F' + \frac{g^2+h^2}{8}R''F'' + \frac{g^3-h^3}{3(g+h)}R'F'''\right.$$

$$\left. + \frac{g^3+h^3}{12(g+h)}RF''''\right] + \ldots\ldots \qquad (8)$$

where R', R'', and R''' are partial derivatives of R with respect to x. The first term of Eq.(8) is proprtional to (h-g) and vanishes when g=h.

(D) Truncation Error for Supersonic Flow on Nonuniform Grids

The full potential equation for the supersonic domain is written as

$$(\bar{R}(F_x)_x + (R(F_y)_y) = 0 \qquad (9)$$

where $\bar{R}$ is the upwind approximation for R in the supersonic domain. The upwind shifting of density is adopted to stabilize the iterative scheme for Eq.(9). Upwind density is given as

$$\bar{R}_{i-1/2} = wR_{i-3/2} + (1-w)R_{i-1/2} \qquad (10)$$

where w is a upwind-shiftirg parameter.

By writing

$$\bar{R}_{i-3/2} = R_{i-1/2} - \Delta xR'_{i-1/2}$$

where

$$\Delta x = x_{i-1/2} - x_{i-3/2}$$

Eq.(10) becomes

$$\bar{R}_{i-1/2} = R_{i-1/2} - w\Delta xR'_{i-1/2} \qquad (11)$$

Then, the first term of Eq.(9) becomes

$$(\bar{R}(F_x))_x = (R(F_x))_x - w\Delta x(R'(F_x))_x$$

Since the first term of Eq.(12) is identical to that analyzed in (C), the truncation error of the first term is given by Eq.(8). The second term on the right side of Eq.(12) is the truncation error caused by upwind shifting of fluid density. The total truncation error of the supersonic domain is therefore written as

$$TE(x) = TE_o(x) + TE_{uw}(x) \tag{13}$$

where $TE_o(x)$ is the truncation error that occurs when no upwind shifting of density is used and given by Eq.(8), and $TE_{uw}(x)$ is equal to the second term of Eq.(12):

$$TE_{uw}(x) = -w\Delta x(R'(F_x))_x \tag{14}$$

3. NUMERICAL EVALUATION OF TRUNCATION ERROR AND OTHER QUANTITIES OF THE FLOW SOLUTION ON THE INITIAL GRIDS

Numerical evaluation of the truncation error formulas derived above is of interest because they may be used as means to evaluate the quality of the grids used and as grid spacing control (GDC) function. It should be noticed, however, that the formulas derived above are expressed in terms of the exact flow solution. In the practice of adaptive grid generation and the flow solution on them, the only way of the numerical evaluation is to use, in the truncation error equations, an numerical (or approximate) solution on the initial grids in place of the exact solution. Therefore, the trncation error estimated by using the finite difference solution is subject to the error of the solution which are caused by the truncation errors of on the initial grids. Furthermore, the estimated truncation error is influenced by the nonlinear nature of the full potential equation where R is a function of the solution. (It should be noticed that, in the previous section, R is assumed to be known exactly.)

In spite of this limitation we attempt to estimate the truncation error of the numerical solution of the flow solution. Instead of using the truncation equations derived above, the truncation is evaluated directly by

$$TE(x) = \delta R \delta F/\delta x^2 - \partial R \partial F/\partial x^2 \qquad (15)$$

where the second term is evaluated by the 5-point difference approximation which is fourth-order-accurate.

The full potential equation was first solved on the initial grids, plotted in Fig. 1, in which 41 grids are uniformly spaced along the wing. The airfoil was assumed to be a parabolic arc airfoil with 10% thickness ratio. In order to avoid the use of a coordinate transformation, the airfoil was represented by the boundary condition on the bottom straight line written as

$$\partial F/\partial y = f(x)M \qquad (16)$$

where f(x) is the surface profile of the airfoil, and M is the Mach number. Equation (15) is a crude approximation of the boundary condition, but sufficient as a computational model for the present study since all the calculations hereafter are performed by using the same model. The difference equations for the full potential equations were iteratively solved by using the AF1 scheme [6].

The following quantities of the initial flow solution, including the truncation error, all along the wing surface were calculated and plotted in Fig. 2.

a) CP (pressure coefficient) distribution

b) An estimate for the truncation error of the difference approximation

c) Second derivative of the flow potential distribution

d) Truncation error due to upwind shifting of fluid density, $|TE_{uw}(x)|$

e) The space derivative of the fluid density along the airfoil surface

Figure 2-A is the CP distribution. Figure 2-B is the truncation error $|TE(x)|$ along the airfoil surface. $|TE(x)|$ jumps up at the grid next to the leading edge, but decreases quickly as x is increased until x=0.25 is reached, and then increases because of the effect of upwind shifting of the flow density. The peaks around x=0.7 are due to the shock. After

reaching a bottom at around x=0.8, |TE| increases toward the trailing edge becuase of the increasing negative gradient of the airfoil. Figure 2-C shows $|F_{xx}|$ along the airfoil surface. $|F_{xx}|$ has a great similarity to |TE| except in approximately $0.25<x<0.7$ where the supersonic bubble and shock are located. Figure 2-D shows the truncation error due to the upwind snifting of the density. Figure 2-E is $|\partial R/\partial x|$ along the airfoil, which shows its high sensitivity to the location of shock.

Very small values of |TE(x)| of Fig. 2-B in the range $0.1<x<0.25$ and around x=0.8 seem to indicate that in these areas much greater grid spacing than in the initial grids may be used. The two peaks of |TE(x)| adjacent to the leading and trailing edge, which are due to the highest curvature of the airfoil at the edges, are indicative of the need of finer grids toward the edges. The two highest peaks at about x=0.7 due to the shock can not be interpreted simply as the truncation error because of the strong nonliiear nature of the full potential equation across the shock, but should be rather interpreted as an indicator of the shock location which demands finer grids.

One might ask if the adaptive grids that will yield a levelized |TE(x)| can be considered as an optimized adaptive grids (or at least as better grids than the initial grids). A part of the answer will be sought in the next section.

4. EFFECT OF DIFFERENT GRID SPACING CONTROL FUNCTIONS ON ADAPTIVE GRIDS AND FLOW SOLUTIONS

Effects of using different quantities obtained from the initial flow solution as the GDC function, with or without modifications, on the adaptive grids generated and the flow solution are studied in this section. The procedure of generating adaptive grids along the airfoil surface is first described.

Assuming that only the grids along the airfoil surface are regenerated by the adaptive grid generation procedure, two functions are defined as

S(x): grid density control (GDC) function

$\psi(x)$: grid density function

where x is the coordinate along the airfoil surface. The GDC function is a function that carries such information of the initial flow solution as the locations of the supersonic bubble, the shock, and areas of high acceleration and deceleration. The grid density function is a function that specifies the density of grids as a function of x, and is inversely proportional to the grid spacing.

The two functions defined in the above paragraph are related by

$$-\frac{d^2}{dx^2}\psi(x) + \sigma\psi(x) = S(x) \qquad (17)$$

$$\psi'(0) = \psi'(1) = 0$$

where σ is a control parameter, x=0 and x=1 are the leading edge and trailing edge of the airfoil, respectively. The above equation is solved by finite difference approximations using the tridiagonal solution scheme once S(x) is specified. Then, the coordinates of the grids along the airfoil surface are obtained by

$$x_k = T^{-1}(k/K), \qquad k=0,1,2,\ldots K \qquad (18)$$

where K is the total number of grid intervals on the airfoil surface, and k is a grid number counted from the leading edge. In the above equation, T(x) is given by

$$T(x) = c\int_0^x \psi(s)ds \qquad (19)$$

where c is a normalizing constant to let T(1)=1.

Equation (16) may be considered as a tranformation of S(x) into $\psi(x)$. The purpose of this transformation is to smooth out any abrupt change in S(x) in order to avoid a sudden change of spacing of adaptive grids. The control parameter σ determines the intensity of the smoothening effect. As σ is increased, ψ becomes more and more similar to S(x), thus the smoothening effect disappears. On the other hand, a very small value will

information carried by S(x).

In the remainder of this section, the results of five case studies using different GDC functions are discussed.

Case 1

The adaptive grids were generated by using |TE(x)| as the GDC (grid density control) function shown in Fig. 2-B, on which the flow equation was solved. In Figure 3, the CP distribution on the adaptive grids are compared with that on the initial grids. The adaptive grids generated along the wing are shown in Fig. 3 by tick marks along the horizontal coordinate line at the bottom of the figure.

In the adaptive grids thus generated, grids are strongly clustered toward the leading and trailing edges as well as around the shock. On the other hand, the grids (in $0.1<x<0.25$) that are between the leading edge and the supersonic region and the grids (in $0.8<x<0.9$) between the shock and the trailing edge became coarse. The strong clustering in the three areas are resulted by the peaks of |TE(x)| of the flow solution on the initial grids near the leading and trailing edges as well as at the shock. At the same time, the coarse grids in the other two areas are due to very small values of |TE(x)| as seen from Fig.2-B (see the line with lozenge marks).

A comparison of the two CP distributions in Fig. 3 suggests several effects of the grid spacings on the flow solution. Coarser grids in the subsonic region after the leading edge causes more expansion of the fluid than on finer grids (CP distribution on the adaptive grids in $0.1<x<0.25$ are higher than that on the initial grids, where the adaptive grids are coarser than the initial grids). The CP distribution at the shock on the adaptive grids are much sharper than that on the initial grids. The expansion of the fluid before the shock in the range of $0.5<x<0.6$ on the adaptive grids are suppressed compared with that on the initial grids. This is attributed to the coarser grids in this area of the adaptive grids than those on the initial grids. The coarser grids in the supersonic domain results in using a higher fluid density in the difference equation because of the upwing shifting of the density in the supersonic region. However, fine grids just before the shock caused an opposite effect of the

upwind shifting that results in a faster expansion of the fluid.

Case 2

|TE(x)| is used as the GDC function just as in Case 1 except it is modified so as to decrease the strength of clustering and to increase the grid density in the coarse grid area. The GDC function is defined as follows:

$$\begin{aligned} S(x) &= |TE(x)| \quad \text{if} \quad 0.5<|TE(x)|<0.0; \\ &= 0.5 \quad \text{if} \quad |TE(x)|>0.5 \\ &= 0.01 \quad \text{if} \quad |TE(x)|<0.01 \end{aligned} \tag{20}$$

The CP distribution on the adaptive grids is compared with that of the initial solution in Fig. 4-A. Although expansion and contraction of grids became much milder than in the previous case, it is still seen that (1) a rapid expansion of grid spacing around 0.1 to 0.25 causes an increase in CP on the graph, and (2) a rapid contraction of grid spacing toward the shock causes a lower CP on the graph. Figure 4-B shows a comparison of |TE(x)| between the initial solution and the adaptive grid solution. It is noticed from this figure that |TE(x)| in the range of $0.1<x<0.25$ for the adaptibe grid flow solution is still very small despite the discrepancy in CP. This indicates that the |TE(x)| is insensitive to the change of physically important quantities of the flow solution.

The results of both Case 1 and the present Case 2 show that estimated truncation error distribution is a poor indicator of the error of the solution, particularly for the error of the CP distribution.

Case 3

The adaptive grids are generated using $|F_{xx}(x)|$ shown in Fig. 2-C as the GDC function. Since $|F_{xx}|$ has sharp peaks near the leading and trailing edges, the grids shown in Fig. 5 are strongly clustered toward the leading and trailing edges. The $|F_{xx}(x)|$ has a peak at the shock, which causes a clustering at the shock. The grid density at the shock becomes even coarser than that on the initial grids at the shock because of much stronger clustering effects at the leading and trailing edges.

The CP distribution on the adaptive grids shown in Fig. 5 looks poor.

The same effect of coarseness on the CP distributions as seen before are observed. A rapid expansion of grid spacing in the subsonic domain causes an upward shifting the the CP distribution, while coarse grid in the supersonic domain causes a downward shifting of CP and smearing of the shock.

The use of $|F_{xx}(x)|$ results in a poor accuracy as a whole because the strong clustering toward the leading and trailing edges causes a lower grid density in all other areas.

Case 4

$|\partial R/\partial x|$ is used as the GDC function. The CP distribution on this choice of the GDC function and the adaptive grids generated are shown in Fig. 5. With this choice, the adaptive grids are moderately clustered toward the leading and trailing edges, while the grids around the shock are strongly clustered. No particular clustering is seen in the supersonic bubble. Coaser grids in both subsonic and supersonic expansion region causes the same effects as seen in the previous cases.

Case 5

The GDC function is set as

$$S(x) = M^2(x) \tag{21}$$

where M is the Mach number, except modified at the leading and trailing edges, and the shock as

$$S(x) = 2M^2(x) \tag{22}$$

The purpose of the modification by Eq.(22) is to enhance the clustering effect at the shock. Figures 7-A, 8-A, and 9-A are the CP distributions on the adaptive grids using 41, 31 and 21 grids along the airfoil surface, respectively. They are compared to the CP distribution on the initial grids. Each of Fig. 7-B, 8-B and 9-B shows the $|TE(x)|$ distributions corresponding to the two CP distributions in Figs. 7-A, 8-A and 9-A, respectively.

The grids generated with the present choice of the GDC function yields smooth changes of grid spacing. Each of Figs. 7-A, 8-A, and 9-A shows that the shock becomes better represented on the adaptive grids than on the equally spaced initial grids, while coarser grids upwind of the shock little affect the CP distribution. The disagreement of the CP distribution downwind of the shock between the initial flow solution and the adaptive grid flow solution is attributed to the change of the CP distribution at the shock.

A comparison of the CP distributions of Fig. 7-A to those in Fig. 9-A is instructive. Even though the grids in Fig. 9-A are coarser than those on Fig. 7-A, the CP distributions upwind the shock agree well. Although the coarser grids in Fig. 9-A causes more expansion upwind of the shock than in Fig. 7-A, the difference is smaller than the discrepancies caused by a rapid change of grid spacing as seen in the previous cases.

5. EFFECT OF GRID SPACING IRREGULARITY ON THE FLOW SOLUTION

During the case studies in the previous section, it was identified that a sudden change of grid spacing may cause a kink in the CP distribution. This is considered as the effect of the first order truncation error in Eq.(8) due to nonuniformity of grid spacing.

In order to study the effect of irregularity of the grids quantitatively, the flow solution was repeated with equally spaced grids except that only one of the grids along the airfoil surface is moved backward or forward at a time. In all calculations for this study, only 21 grids are used along the airfoil.

Figure 10 shows two CP distributions, where the third grid counted from the leading edge is moved half way forward or backward to the next grid as marked by lozenge and circular marks at the bottom of Fig. 10. This figure shows that moving a grid backward (see lozenge marks) causes an upward deviation of the CP curve on the moved grid while the CP on the adjacent grid upwind is deviated downward.

Figure 11 shows similar results of moving the 10th grid, which is

located in the supersonic flow domain. The deviations caused by the move show almost the same trend as seen in Fig. 10, namely the forward shift of a grid causes a a upward shift of CP on the graph at that grid, while the backward shift causes a downward shift of CP on the graph.

Figure 12 shows the results for the 18th grid moved. The deviation of the CP distribution caused by the move is opposite to those seen in Figs. 10 and 11, suggesting that the direction of the CP deviation depends on whether the grid is in a expanding flow or in a contracting flow.

6. CONCLUSIONS

This paper described the results of the study on (i) the analytical expressions for the truncation error of the transonic full potential equation, (ii) numerical study of the estimated truncation error, (iii) adaptive grid generation using various different quantities obtained from the initial flow solution, and (iv) effect of irregularity of grid spacing on the flow solution.

The estimated truncation error does not seem to represent the error of the flow solution adequately, thus is not suitable as a grid density control (GDC) function for adaptive grid generation. Among several different quantities taken from the initial flow solution, the M^2 distribution is found to be most useful with a modification to enhance the clustering at the shock.

One important fact learned quantitatively through the numerical study is that a rapid change of grid spacing is damaging to the accuracy of the flow solution. This means that, while the objective of adaptive grids is to dispatch a larger number of grids to where the error is high, the grid density should be only gradually changed from the low error area to the high error area. The need of gradual change of grid density justifies the use of the diffusion process for the GDC function proposed by the author.

The practice of a mathematical optimization of grid distribution for the full potential equation does not seem to feasible, because of the complex nature of the relation among an error estimate, grid spacing and the real error of the flow solution. For further research, it is rather recommended to develop empirical relations between the CP distribution and

the required grid spacing distribution as well as the acceptable rates of grid spacing change.

REFERENCES

[1] Holst, T. L. and Brown, D.,"Transonic Calculations Using Solution-Adaptive Grids," AIAA 5th Computational Fluid Dynamics Conference, Palo Alto, California, June 22-23, 1981

[2] Nakamura, S. and Holst, T. L. "A New Solution Adaptive Grid Generation Method for Transonic Airfoil Flow Calculations," NASA-TM 81330, Oct., 1981

[3] Ushimaru, K., "Development and Application of Adaptive Grids in Two-dimensional Transonic Calculations," AIAA/ASME 3rd Joint Thermophysics, Plasmas and Heat Transfer Conference, St. Louis, Mi., June 7-11, 1982

[4] Anderson, D. A., and Rai, M. M., "The Use of Adaptive Grids in Solving Partial Differential Eqations," in Numerical Grid Generation, North-Holland, 1982

[5] Mastin, C. W., "Error Induced by Coordinate Systems," in Numerical Grid Generation, North-Holland, 1982

[6] Ballhaus, W. F., Jameson, A., and Albert, J., "Implicit Approximate-Factorization Schemes for the Efficient Solution of Steady Transonic Flow Problems," NASA-TM X-73,202, 1977

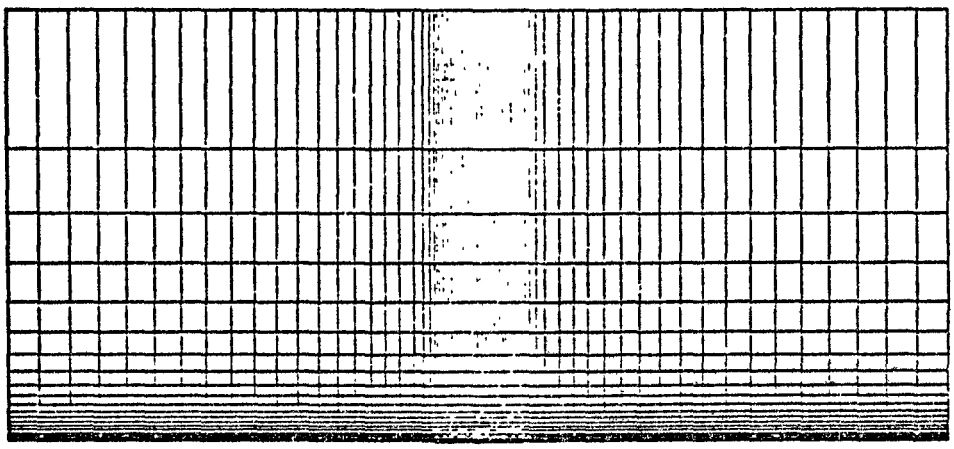

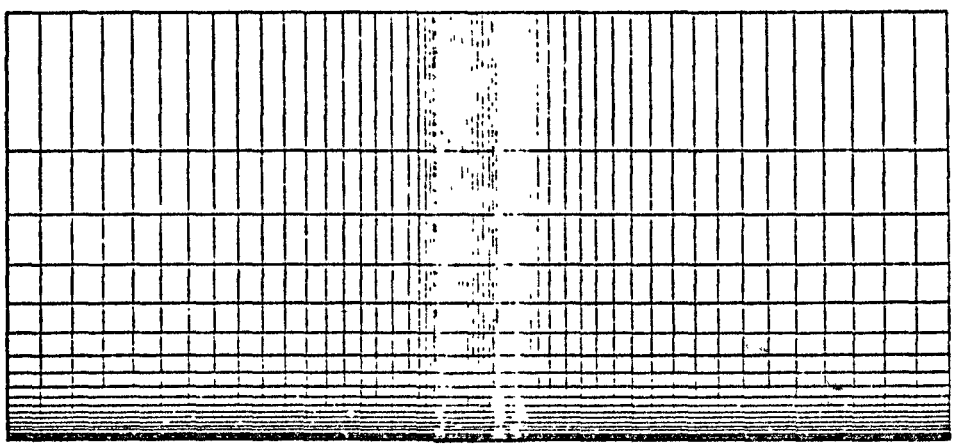

Figure 1 Illustration of Sample Grids

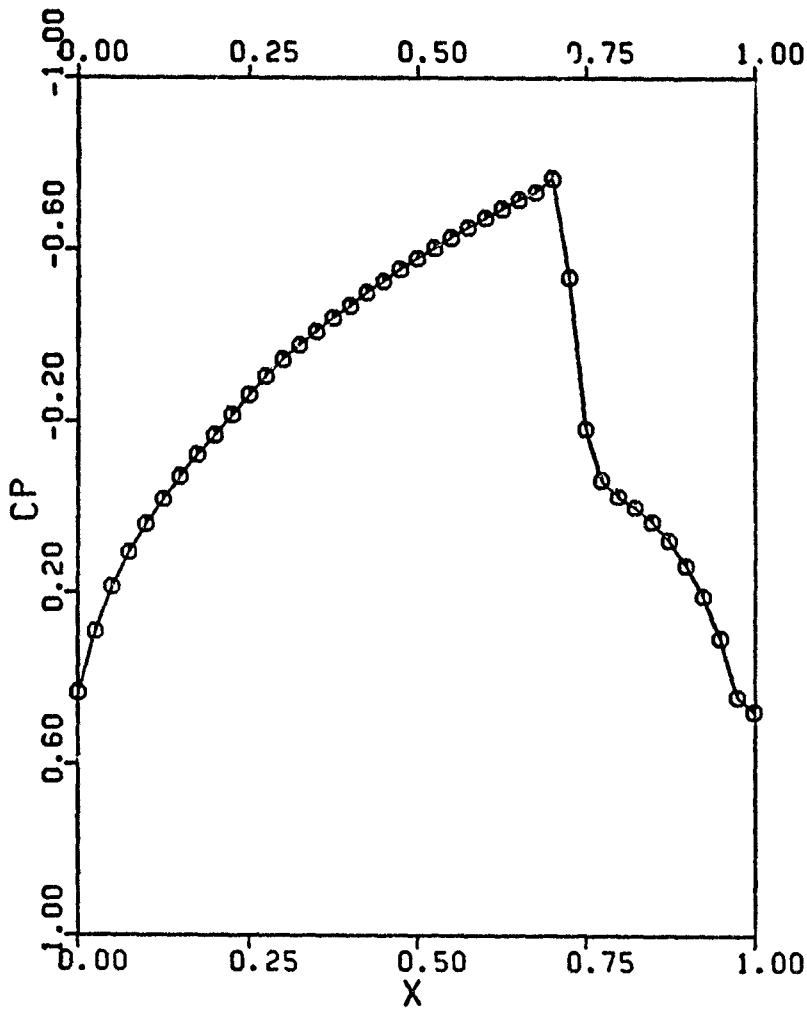

FIGURE 2-A PRESSURE COEFFICIENT
(41 equally spaced grids)

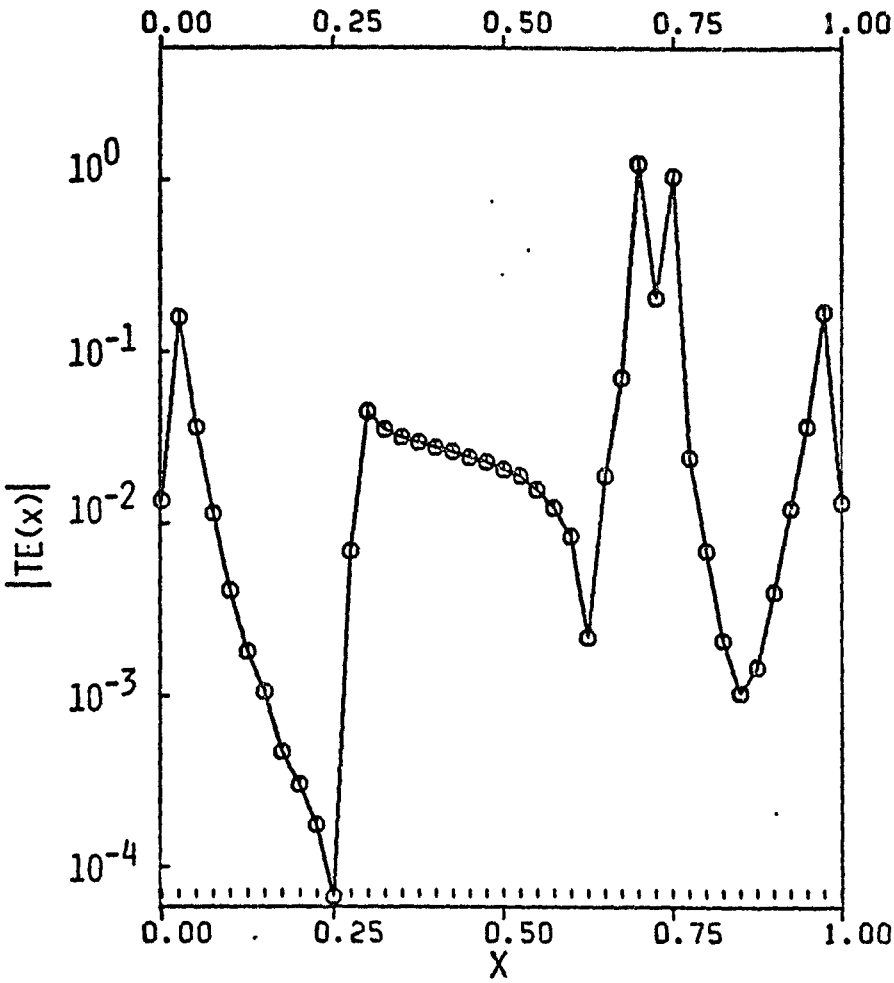

FIGURE 2-B DISTRIBUTION OF |TE(x)|

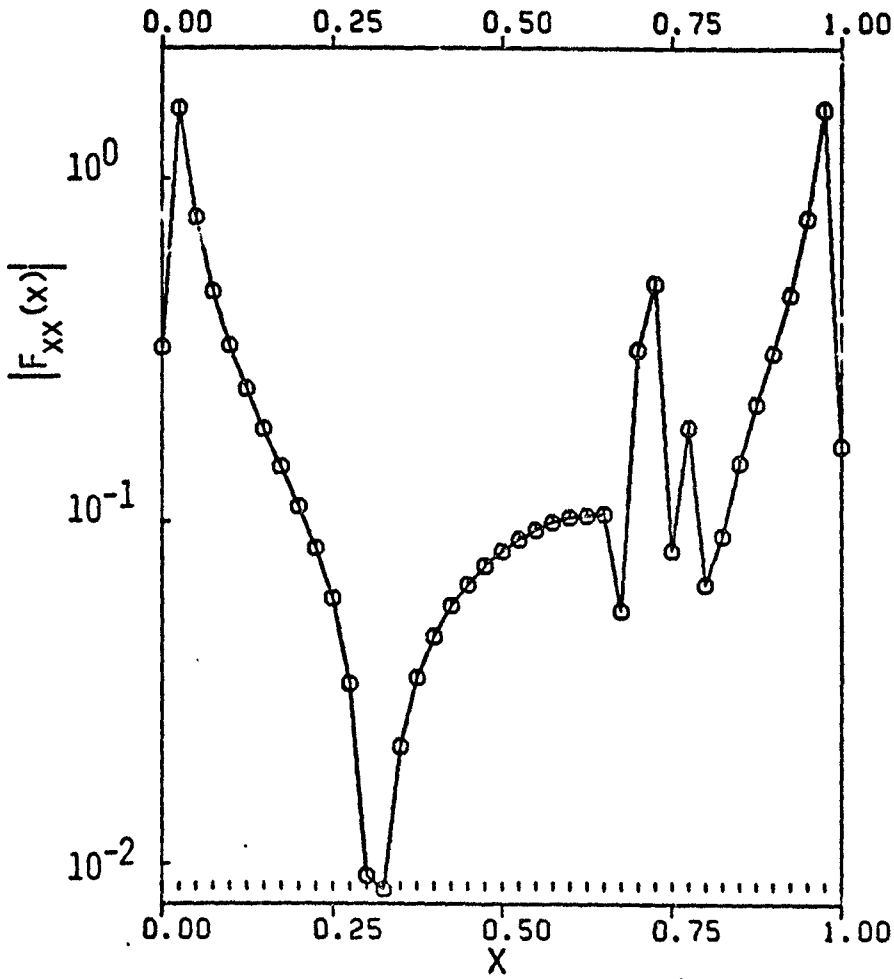

FIGURE 2-C DISTRIBUTION OF $|F_{XX}(x)|$

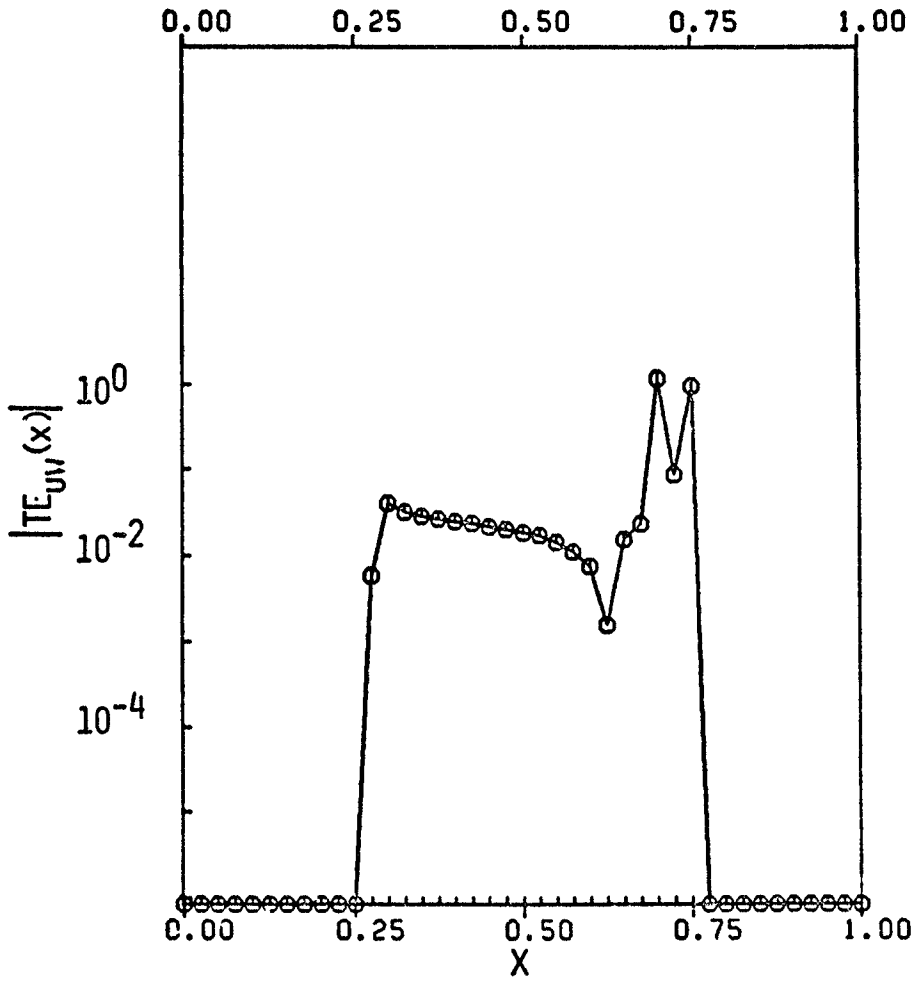

FIGURE 2-D ESTIMATED TRUNCATION ERROR DUE TO UPWIND SHIFTING OF DENSITY

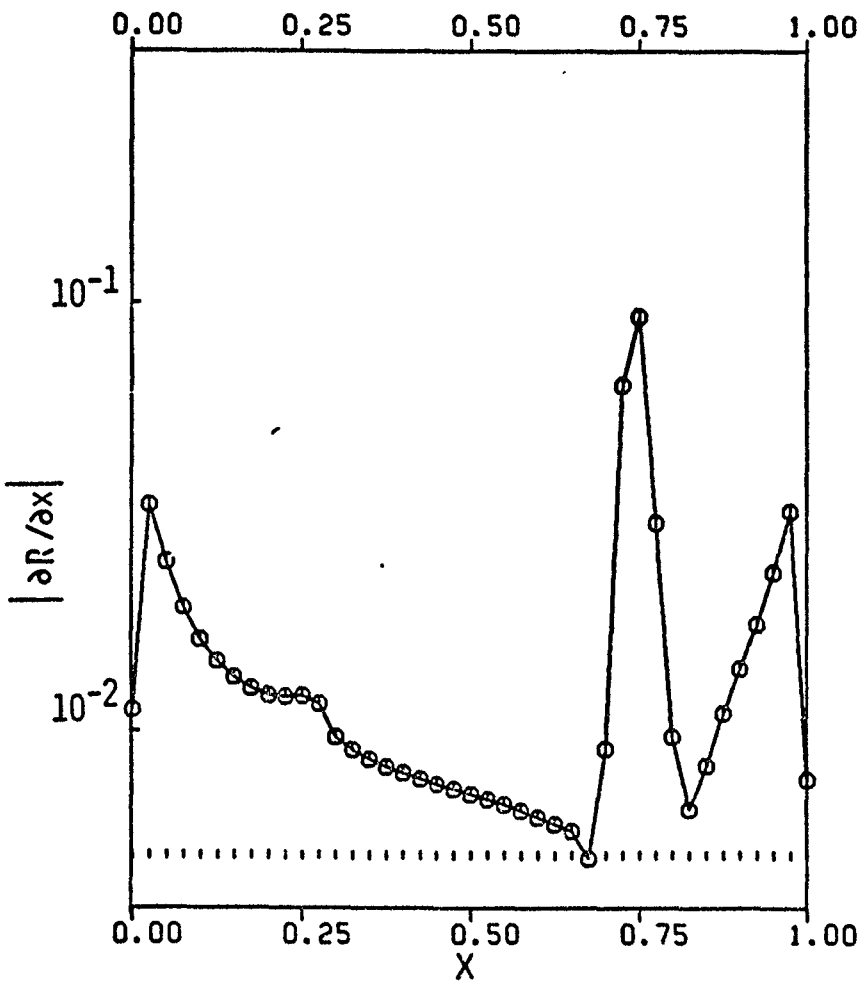

FIGURE 2-E DISTRIBUTION OF $|\partial R/\partial x|$

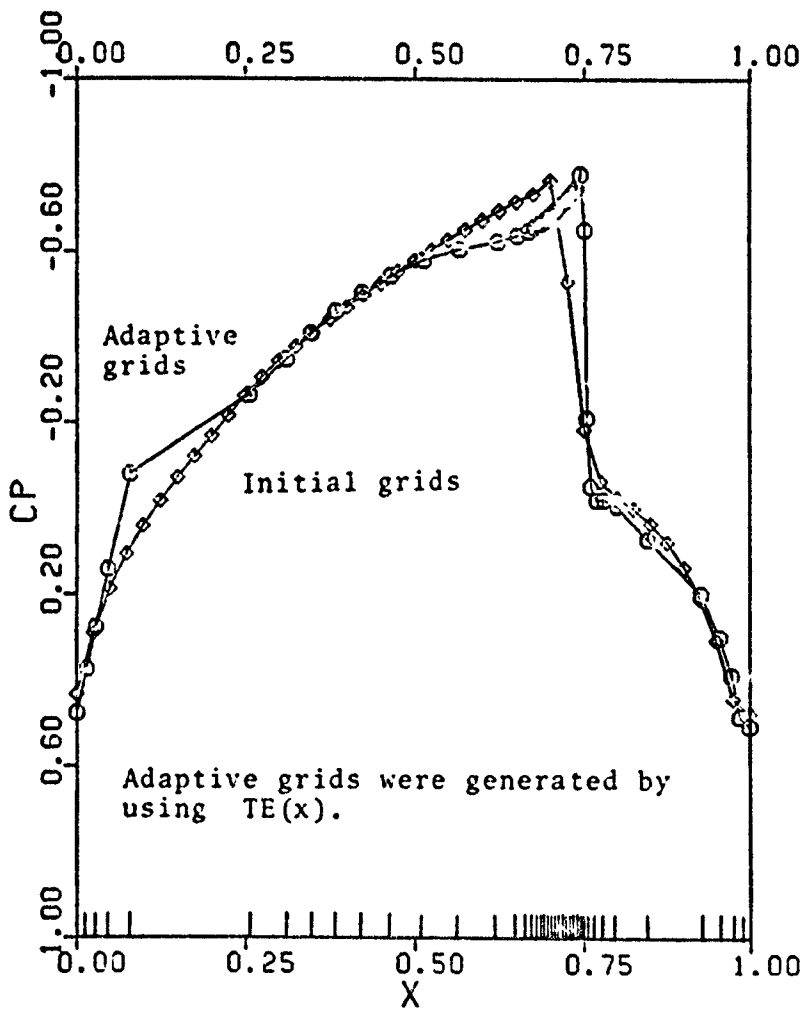

FIGURE 3 PRESSURE COEFFICIENT, CASE 1

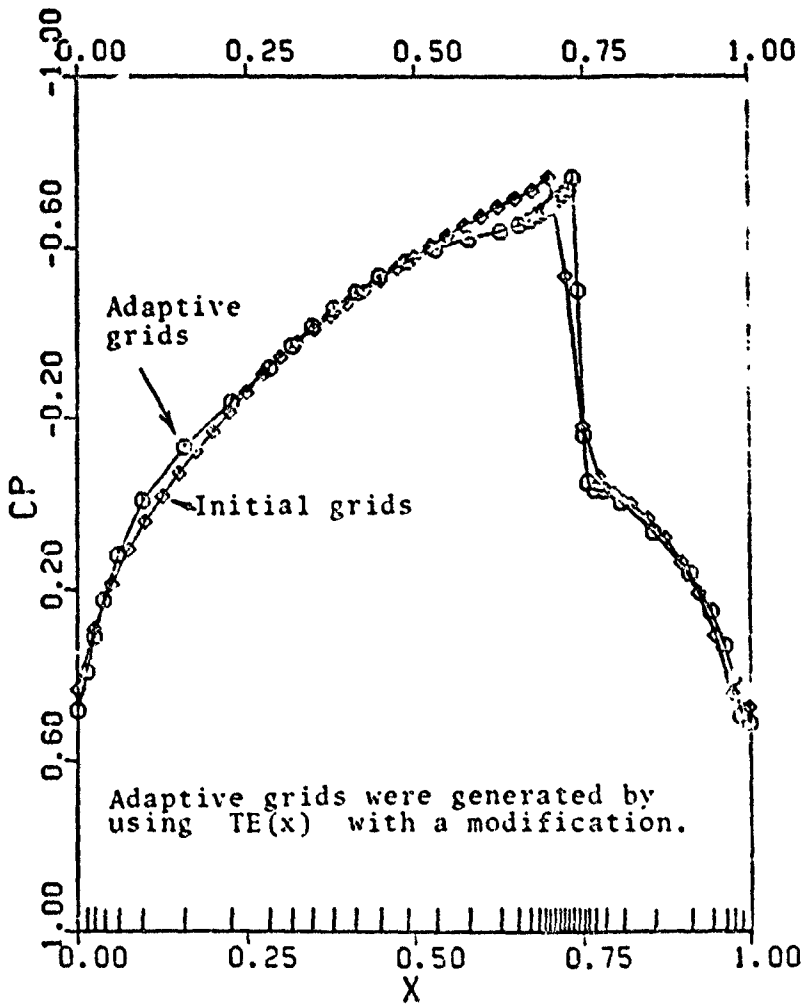

FIGURE 4-A PRESSURE COEFFICIENT, CASE 2

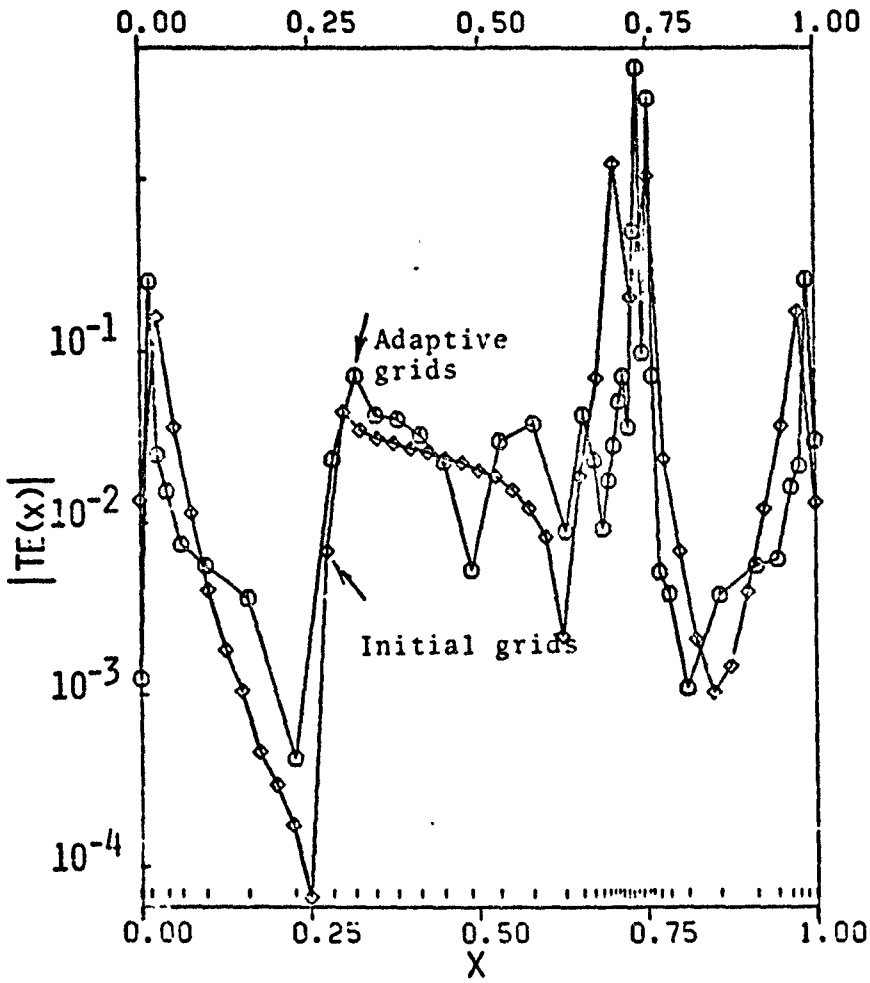

FIGURE 4-B ESTIMATED TRUNCATION ERROR, CASE 2

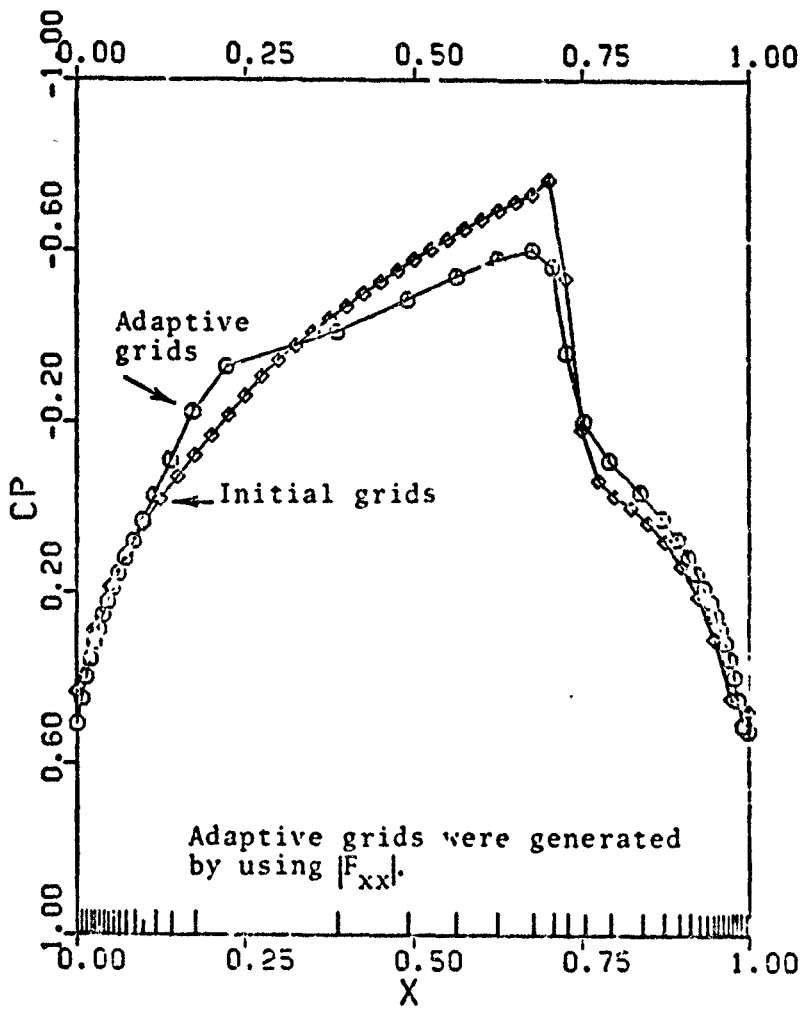

FIGURE 5 PRESSURE COEFFICIENT, CASE 3

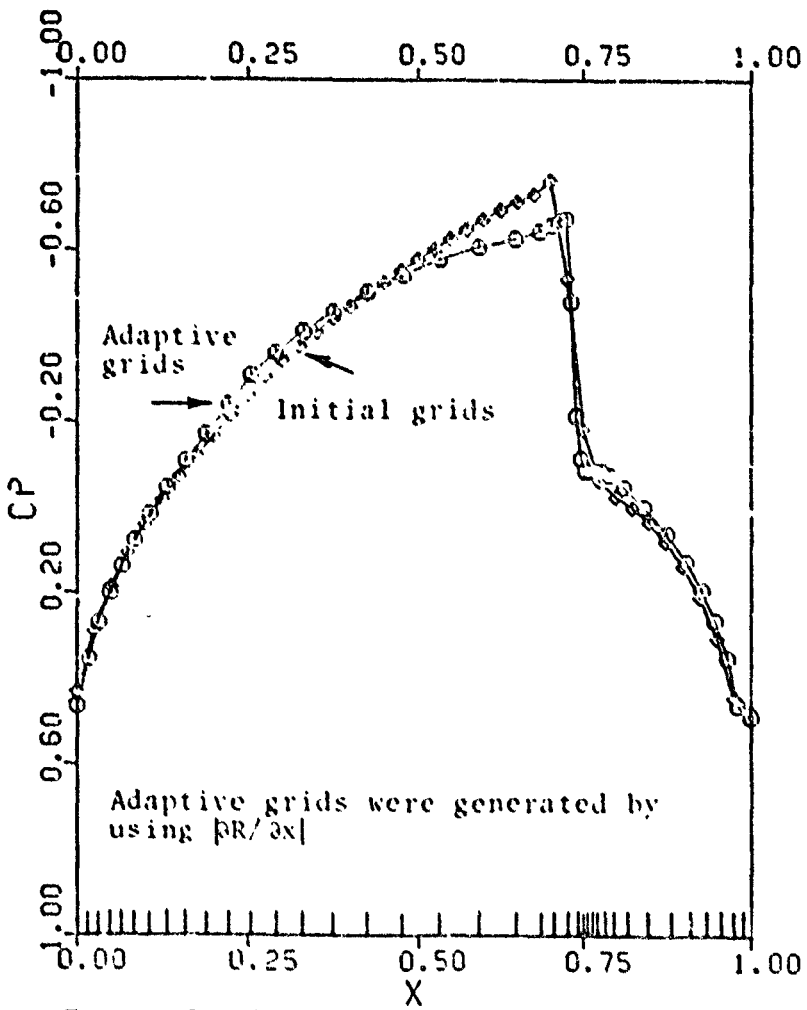

FIGURE 6 PRESSURE COEFFICIENT, CASE 4

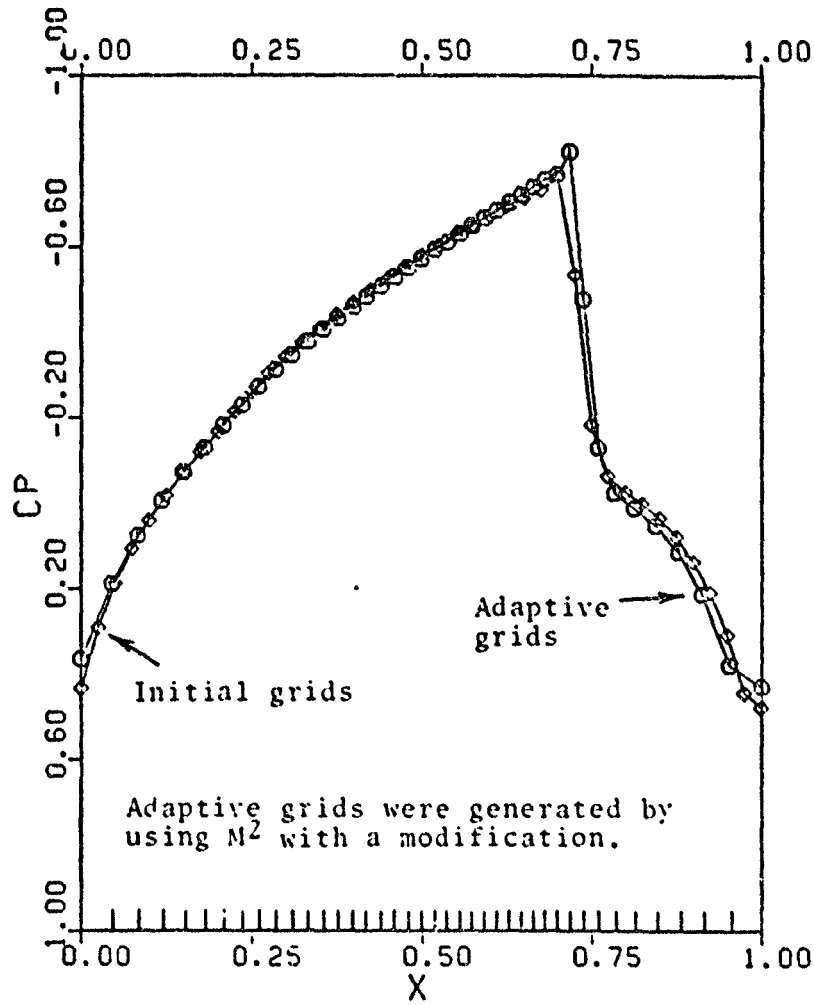

FIGURE 7-A PRESSURE COEFFICIENT, CASE 5
(41 grids)

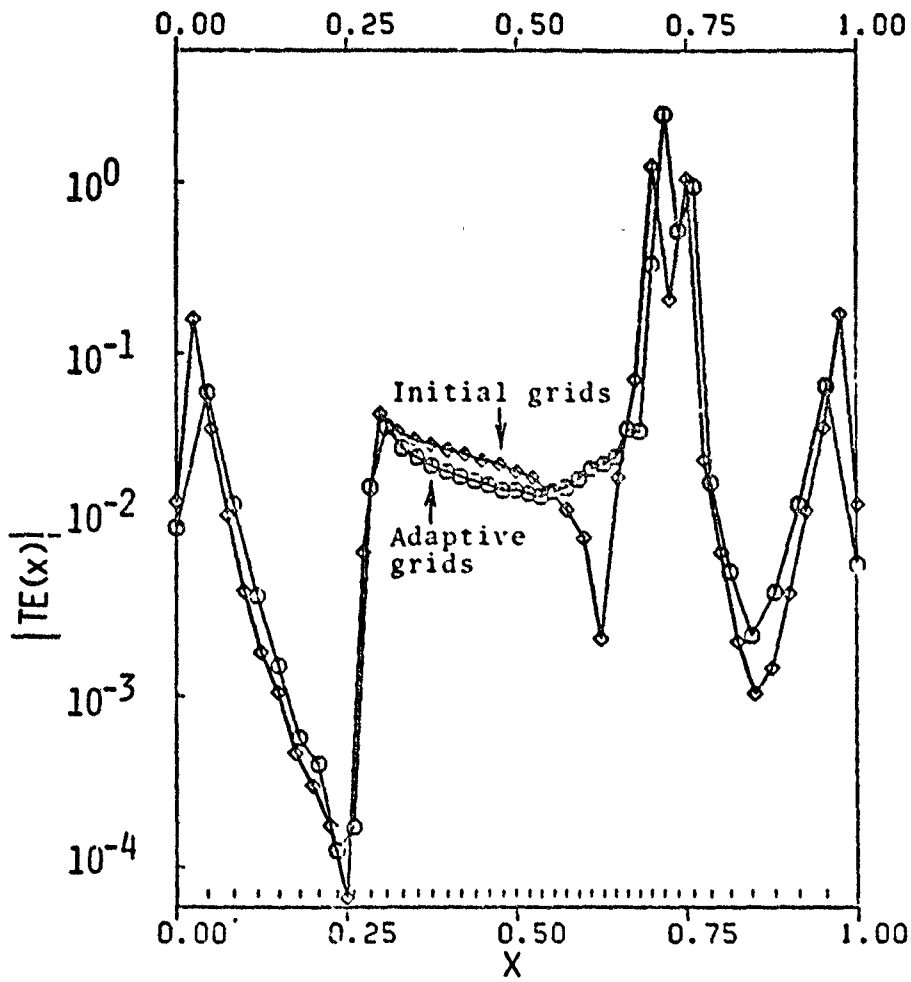

FIGURE 7-B ESTIMATED TRUNCATION ERROR, CASE 5
(41 grids)

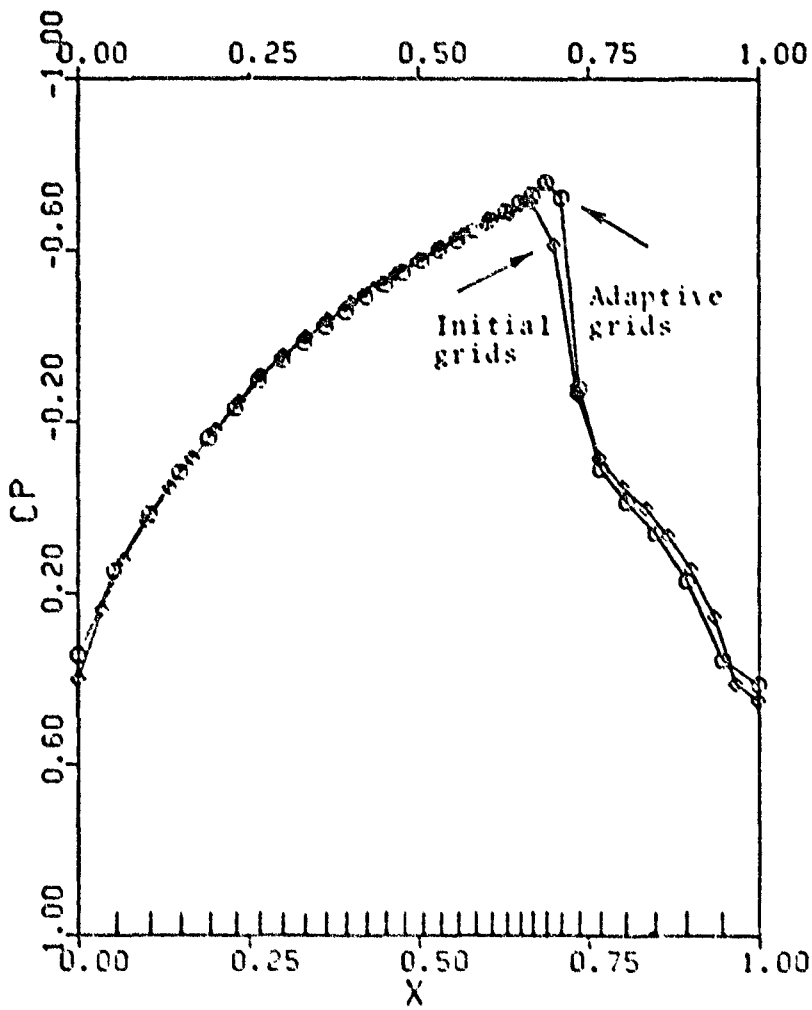

FIGURE 8-A PRESSURE COEFFICIENT, CASE 5
(31 grids)

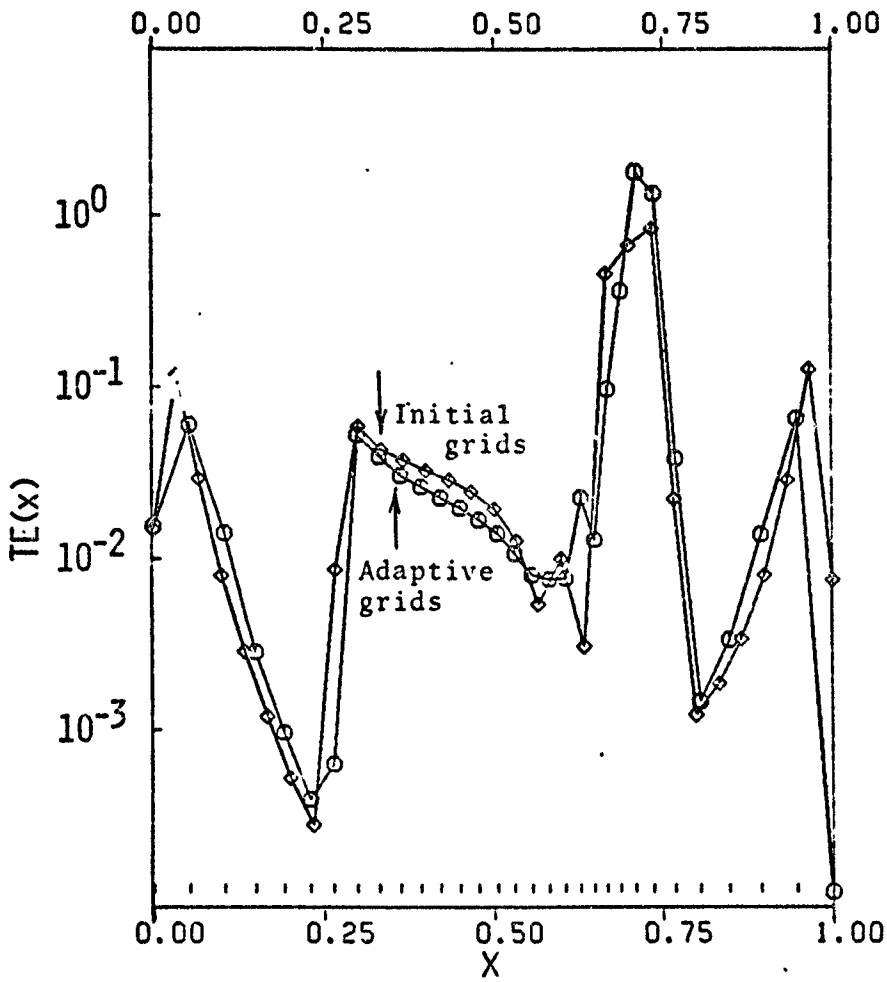

FIGURE 8-B ESTIMATED TRUNCATION ERROR, CASE 5
(31 grids)

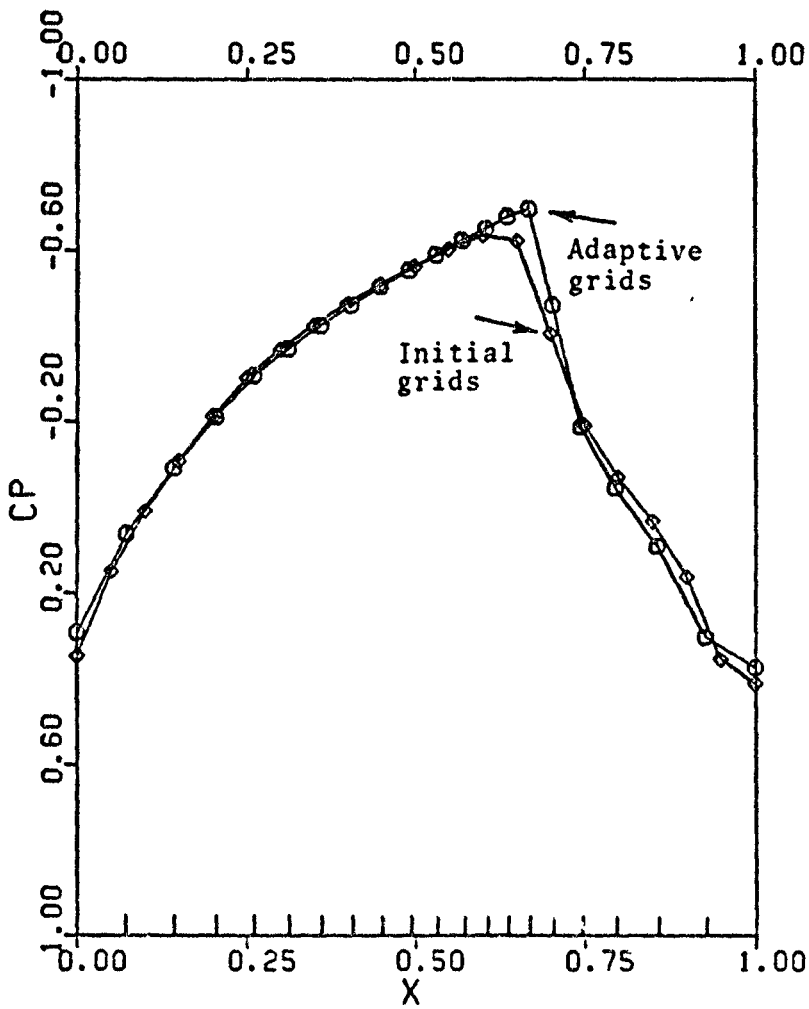

FIGURE 9-A PRESSURE COEFFICIENT, CASE 5
(21 girds)

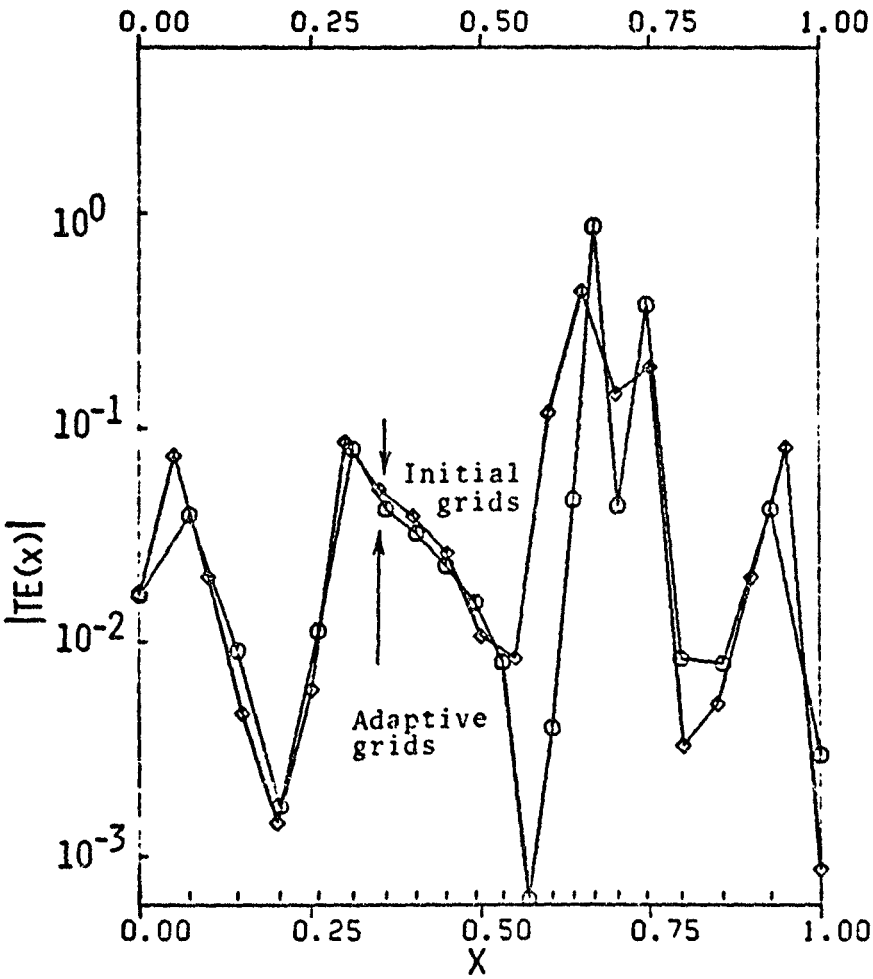

FIGURE 9-B ESTIMATED TRUNCATION ERROR, CASE 5
(21 grids)

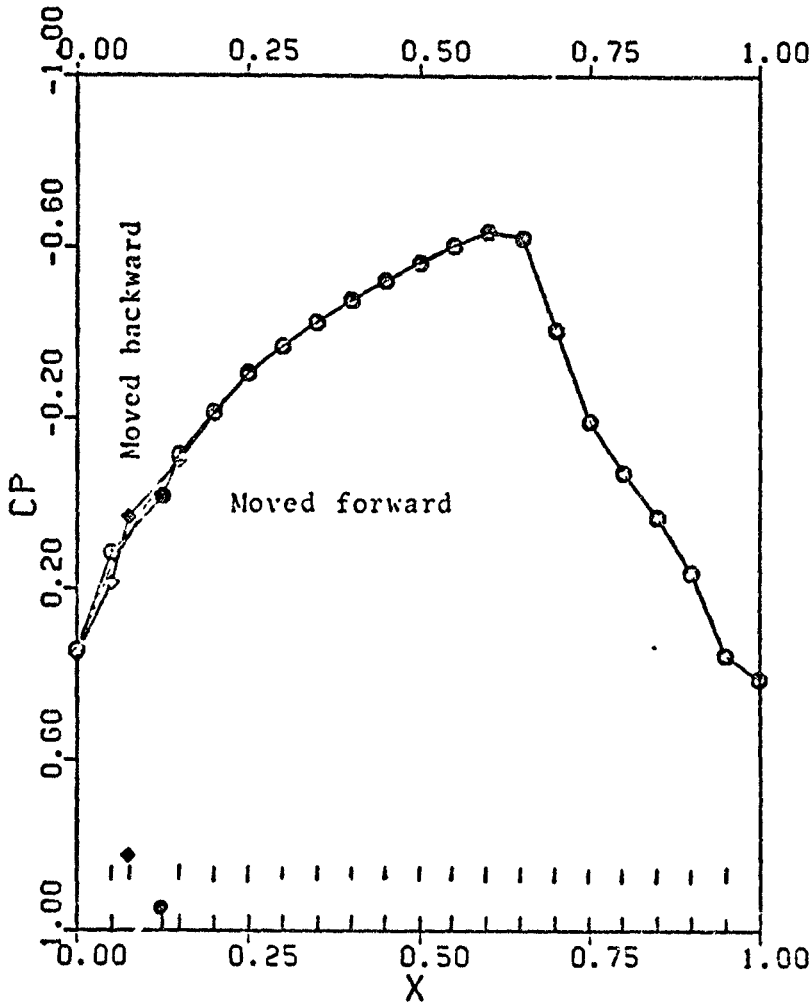

FIGURE 10 EFFECT OF THE 3RD GRID MOVED

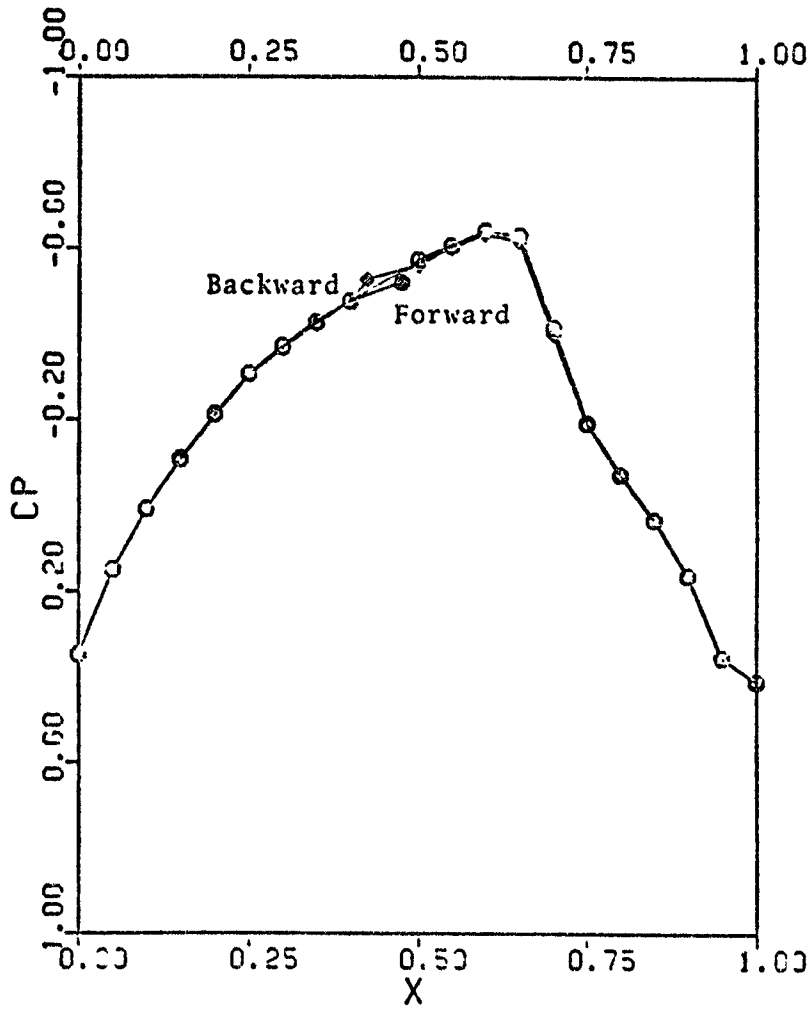

FIGURE 11 EFFECT OF THE 10 GRID MOVED

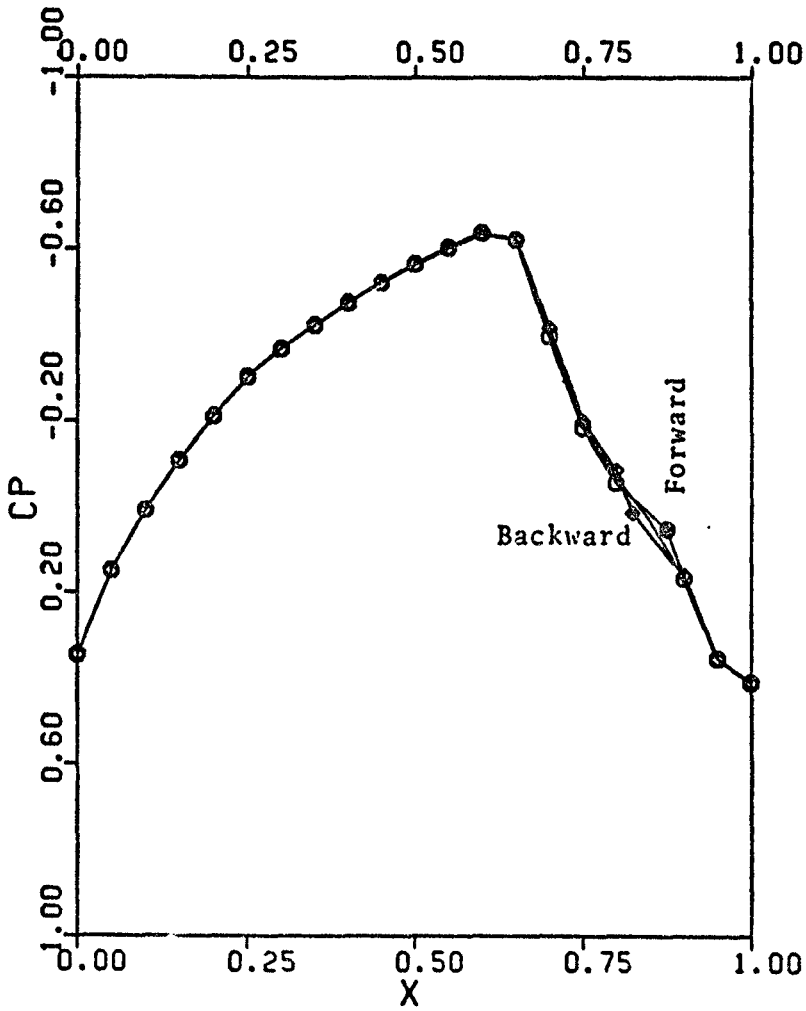

FIGURE 12 EFFECT OF THE 18TH GRID MOVED

End of Document